Neuronal Nitric Oxide Synthase Ligand and Protein Vibrations at the Substrate Binding Site. A Study by FTIR†

W. John Ingledew,*,‡ Susan M. E. Smith,§ John C. Salerno,§ and Peter R. Rich||

School of Biology, University of St. Andrews, St. Andrews KY16 9JF, U.K., Department of Biology, Rensselaer Polytechnic Institute, Troy, New York 12180, and Glynn Laboratory of Bioenergetics, Department of Biology, University College London, Gower Street, London WC1E 6BT, U.K.

Received November 29, 2001

ABSTRACT: Improvements in sensitivity and data processing of Fourier transform infrared (FTIR) spectroscopy enable it to be used to detect changes in protein structure at the atomic level. This paper reports a study of neuronal nitric oxide synthase (nNOS) by FTIR difference spectroscopy in the 1000−2500 cm^{-1} range where vibrational bands of ligands, prosthetic groups, and protein and amino acid side chains are found. We have exploited the photolyzable CO compound of the ferrous heme of nNOS to produce light-induced CO photolysis difference spectra and to compare spectra after hydrogen/deuterium exchange. In (reduced) *minus* (reduced *plus* CO) difference spectra, negative bands at 1931 and 1907 cm^{-1} are observed due to photolysis of multiple forms of ferrous heme-ligated CO, similar to those observed by resonance Raman spectroscopy [Wang et al. (1997) *Biochemistry 36*, 4595−4606]. Photolysis of the ferrous heme CO compound is accompanied by hitherto unreported changes in the 1000−2000 cm^{-1} region that arise from changes of protein backbone, substrate, amino acid side chain, and cofactor vibrations. Preliminary assignments of vibrations are made on the basis of frequencies and the effects of hydrogen/deuterium exchange, and in the light of known atomic structures.

Nitric oxide synthases (NOS)[1] are widely distributed, and the NO produced is a ubiquitous cell-signalling molecule with central roles in physiology and pathology (*1*−*7*). The NO is produced by the action of NOS on arginine by a two-step NADPH- and O_2-dependent oxidation to citrulline (*8*−*11*). Mammalian nitric oxide synthases form a family of three homologous but distinct isoforms, neuronal (nNOS), endothelial (eNOS), and cytokine-inducible (iNOS), which are functionally distinguished by their regulation (*6*). All three isoforms are active as homodimers (e.g., *12*).

NOS consists of an oxygenase domain and a multidomain reductase linked by a calmodulin binding site that can be split by limited trypsinolysis. The N-terminal oxygenase domain binds iron-protoporphyrin IX (heme B) and tetrahydrobiopterin (H_4B); this region comprises the catalytic core of the molecule (*13*, *14*). The C-terminal reductase domains bind FMN and FAD, and contain the NADPH binding site (*15*).

The NOS oxygenase domains form a distinct family that includes the single-domain prokaryotic NOS enzymes. They are not closely related to other enzymes, and are not homologous to the cytochrome P450 superfamily, which has a superficially similar heme−thiolate site for oxygen chemistry. The reductase domains, in contrast, are closely related to the cytochrome P-450 reductases (*14*−*16*). Crystal structures of the NOS oxygenase domain have been determined for the iNOS and eNOS isoforms (*17*−*20*). The core of the oxygenase domain is made up of several winged β-sheets. From these structures, the residues involved in L-arginine and H_4B binding have been identified, but the reaction mechanism is not fully resolved. The enzyme functions as a dimer with electron transfer occurring between flavin and heme groups located on adjacent subunits in the dimer (*21*). The reaction mechanism and catalytic site have recently been probed by pre-steady-state kinetic analyses using optical and resonance Raman spectroscopy (*22*, *23*). A ferrous dioxygen complex of the oxygenase domain of nNOS is formed in 0.3−3.0 ms after mixing oxygen with the reduced enzyme (stretch of the ν_{O-O} at 1135 cm^{-1}) (*23*). Further structure/function insights have been gleaned using resonance Raman spectroscopy to show that hydrogen bonding between the proximal cysteine and a tryptophan residue modulates the strength of the Fe^{III}−NO bond (*24*).

Improvements in sensitivity and data processing of Fourier transform infrared (FTIR) spectroscopy have enabled the technique to be used to detect changes in protein structure at the atomic level. However, because of the very large number of vibrational bands, difference spectroscopy is used to study changes of a limited number of bands in a region

† This work was funded by grants from the Wellcome Trust (Grant 062827, P.R.R.), The Nuffield Foundation (W.J.I.), and The American Diabetes Foundation (S.M.E.S. and J.C.S.).

* To whom correspondence should be addressed at the Biomolecular Sciences Building, School of Biology, University of St. Andrews, St. Andrews KY16 9JF, U.K. Phone: (44) 1334 463408. Fax: (44) 1334 463400. E-mail: wji@st-andrews.ac.uk.

‡ University of St. Andrews.

§ Rensselaer Polytechnic Institute.

|| University College London.

[1] Abbreviations: FTIR, Fourier transform infrared spectroscopy; NOS, nitric oxide synthase; nNOS, neuronal nitric oxide synthase; eNOS, endothelial nitric oxide synthase; iNOS, cytokine-inducible nitric oxide synthase; NO, nitric oxide; CO, carbon monoxide; H_4B, tetrahydrobiopterin; P-420, inactive form of NOS characterized by a 420 nm band in the hemeII-CO spectrum.

10.1021/bi012101v CCC: $22.00
Published on Web 06/06/2002

of interest. For example, photolysis of the CO and cyanide adducts of ferrous heme a_3 has been used to probe the active site and protonation sites of cytochrome *c* oxidase (*25*−*28*). In this paper, we report the first studies on the full-length nNOS (MW 161K, *29*) by FTIR difference spectroscopy in the 2500−1000 cm^{-1} region. Vibrational bands of ligands, prosthetic groups, and protein and amino acid side chains are reported. Putative assignments have been made in conjunction with effects of D_2O exchange on vibrational bands and in the light of known atomic structures.

MATERIALS AND METHODS

NOS Purification. Rat nNOS was purified from a protease-deficient *Escherichia coli* strain ER2556 transformed with pGROELS and the pCWori+ nNOS vector as described previously (*30*). Cells expressing nNOS were broken using a French pressure cell (7000 psi), and after removal of cell fragments by ultracentrifugation for 70 min at 144000*g*, nNOS was purified from the supernatant by 2′-5′-ADP Sepharose affinity chromatography. nNOS was concentrated to approximately 30 μM and stored at −80 °C in 50 mM Tris buffer, pH 7.4, 0.1 mM dithiothreitol, 0.1 mM EDTA, 500 mM NaCl, 1 mM H_4B, and 2 mM arginine with 10% glycerol. Activity was assessed using the Greiss assay in the 96 well plate format (Gross SS, personal communication), and heme content and integrity of thiolate ligation and ability to bind arginine were assessed spectrophotometrically.

Preparation of FTIR Samples. Prior to sample preparation for FTIR, nNOS was further concentrated using centrifugal concentrators (Vivascience Ltd., Lincoln, U.K.). The nNOS was exchanged into a buffer of 40 mM TES, 20 mM arginine, 2 mM EDTA, 1 mM dithiothreitol, 0.1 mM $CaCl_2$, 1 μM H_4B, and 1% glycerol (pH 7.6). The samples of H_4B- and heme-replete nNOS were prepared for FTIR by pipetting 10 μL of enzyme solution, containing approximately 8 nmol of nNOS, onto a 25 mm diameter CaF_2 window and placing it under a stream of water-saturated CO gas. The sample was then reduced with 2.0 μL of 0.1 M sodium dithionite (in 400 mM TES, 100 mM arginine at pH 7.6, and 10% glycerol). After further exposure to the stream of CO for 1 min, a second CaF_2 window was placed on top, the sample was squeezed to an optimal thickness, and the edges were sealed with Dow Corning MS24 Silicon Compound. Formation of the reduced CO compound was confirmed by optical spectroscopy and by the characteristic hemeFe^{II}·C−O bands at 1931 and 1907 cm^{-1} in the FTIR spectrum.

D_2O Exchange. The nNOS to be exchanged was diluted 10-fold in 40 mM TES, 20 mM arginine, 2 mM EDTA, 1 mM dithiothreitol, 0.1 mM $CaCl_2$, 1 μM H_4B, and 1% glycerol (pD 7.6) in D_2O and reconcentrated using Viascience centrifugal concentrators. This process was repeated 3 times. Samples were then prepared as for H_2O solutions, but with all re-wetting solutions prepared with equivalent D_2O buffers and with a CO stream saturated with D_2O vapor. The pD was measured using a pH electrode and allowing for the offset using standard tables. We used the amide II region of the absolute spectra to estimate the extent of D/H exchange following published methods (*31*, *32*). The amide II band is 60% due to N−H bending (40% C−N stretch) which shifts from 1545 to 1445 cm^{-1} on deutration. The dimunition of the amide II band on deutration is used to calculate the extent of exchange; the exchange is above 85%.

FTIR Photolysis Difference Spectroscopy. FTIR spectra were recorded on a Brüker ISF 66/S spectrometer fitted with a liquid nitrogen-cooled MCT-A detector. The normal acquisition parameters were as follows: aperture, 1.5 mm; phase resolution, 128; phase correction mode, Mertz; apodization function, Blackman-Harris 3-term; zero filling factor, 2; and scanner velocity, 40 kHz. Actinic light was provided by a 250 W quartz-iodine lamp, filtered with glass heat filters, water, and BG39 filters, and delivered to the sample via a light pipe. The sample was water-thermostated at 283 K. Typically 100 interferograms at 4 cm^{-1} resolution were averaged to provide an initial dark baseline; the light was then switched on, and the recording was repeated after a delay of 1 s. Finally, the light was switched off, and the recording was repeated after 2 s dark relaxation time in order to provide an indication of relaxation rate and sample baseline drift. Light/dark cycles were repeated up to 5000 times over periods of up to 3 days to enable signals of 10^{-6} ΔA to be observed with low noise levels. During this time, the samples slowly convert to the inactive P-420 form (420 denotes the λ_{max} of the heme**II**−CO compound, see Results and Discussion). Unless otherwise stated, spectra shown are unligated (i.e., light) *minus* ligated (i.e., pre-illumination dark) difference spectra from which 50% of the final dark baseline drift (i.e., post-illumination dark recording *minus* pre-illumination dark recording) has been subtracted. Visible absorbance spectra of the samples in the CaF_2 windows were obtained with an in-house purpose-built spectrophotometer.

RESULTS

CO Photolysis Difference Spectra in H_2O. Figure 1A shows a static heme**II**−CO photolysis difference spectrum of nNOS in H_2O at pH 7.6 and 283 K. A 50% weighted difference spectrum of dark (post-illumination) minus dark (pre-illumination) has been subtracted in order to remove any baseline drift (Figure 1C), although this had very little effect on the resultant spectra. Positive peaks correspond to features due to the photodissociated enzyme and troughs due to those of CO-bound enzyme. Changes caused by photolysis of the heme-bound CO ligand itself have a major trough at 1931 cm^{-1} and a minor trough at 1907 cm^{-1}. Putative B-states of the CO-ligated form (*33*) are observed weakly as positive features in the 2140 cm^{-1} region; these have been proposed to be due to photolyzed CO that is transiently bound in a different manner. Also seen in Figure 1 is a feature with a peak at 1982 cm^{-1} and a trough at 1967 cm^{-1}; this increases in size as the sample ages, while the 1931 and 1907 cm^{-1} features decrease with aging. This 1982/1967 cm^{-1} feature correlates with the optically detected formation of the inactive 'P-420' form of the enzyme (420 denotes the λ_{max}, in nanometers, of the heme**II**−CO compound of this form of the enzyme). In some samples, detectable levels of the species are present from the start of incubation; in others, the species is initially absent. Its development is more rapid in the absence of arginine, and the long time course of experiments mitigates against obtaining good spectra of nNOS in the absence of substrate. This phenomenon and the protective effects of ligands are well documented in NOS; the P-420 form is inactive (*34*). The time dependence of the development of the 1981/1967 cm^{-1} form allows the spectral resolution of the FTIR spectra of each form by subtraction, and these are shown in Figure 2. Trace F (Figure 2) shows

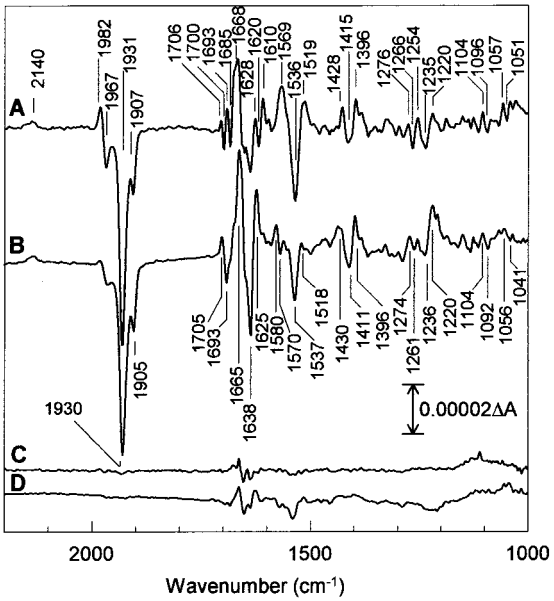

FIGURE 1: Light-induced FTIR difference spectra of CO photolysis in H_2O and D_2O at pH/pD 7.6 and 283 K. (A) nNOS at pH 7.6 in H_2O, light *minus* dark (pre-illumination) difference spectrum from which 50% of the dark (post-illumination) *minus* dark (pre-illumination) control has been subtracted. (B) nNOS in D_2O at pD 7.6, light *minus* dark difference spectrum from which 50% of the dark *minus* dark control has been subtracted. (C) nNOS at pH 7.6 in H_2O, the subtracted dark minus dark control (50% of the dark minus dark spectrum). (D) nNOS at pD 7.6 in D_2O, the subtracted dark minus dark control (50% of the dark minus dark control). Samples of the CO adduct of fully reduced nNOS were prepared in H_2O or D_2O buffers at pH/pD 7.6 as described under Materials and Methods. After sufficient time for equilibration and settling at 283 K, repetitive light/dark cycles were recorded and averaged. Each scan consisted of 100 averaged interferograms at 4 cm^{-1}, and the spectrum shown is an average of 2000 scans. Photolysis was by a 250 W lamp protected by BG39 and water filters. The samples were prepared as described under Materials and Methods.

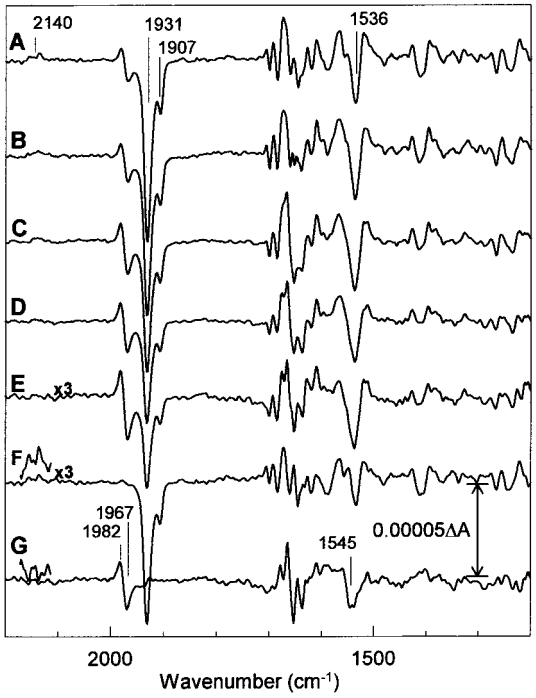

FIGURE 2: Time dependence of the light-induced FTIR difference spectra of CO photolysis in H_2O at pH 7.6 and 283 K. (A) Spectrum taken during the first 8 h of light *minus* dark difference spectrum from which 50% of the dark *minus* dark control has been subtracted (500 scans); (B) spectrum taken during the second 8 h of light *minus* dark difference spectrum from which 50% of the dark *minus* dark control has been subtracted (500 scans); (C) spectrum taken during the third 8 h of light *minus* dark difference spectrum from which 50% of the dark *minus* dark control has been subtracted (500 scans); (D) light *minus* dark difference spectrum from which 50% of the dark *minus* dark control has been subtracted (500 scans) obtained after 30 h; (E) light *minus* dark difference spectrum from which 50% of the dark *minus* dark control has been subtracted (500 scans) obtained after 40 h; (F) the native spectrum, the late spectrum (E) was fractionally subtracted from the early spectrum (A) until the 1982/1967 cm^{-1} feature was minimal; (G) the deconvoluted 'P420' species spectrum. Samples of the CO adduct of fully reduced nNOS were prepared in H_2O buffer at pH 7.6 as described under Materials and Methods, and the conditions were set up as described in the legend of Figure 1.

the corrected 'early' spectrum for nNOS in the presence of arginine, and this is essentially similar (except for the 1981/1967 cm^{-1} feature) to trace A in Figure 1. Figure 2G shows the spectrum of the 'aged' species, which has a clear signature in the CO region and a trough around 1545 cm^{-1}.

The ratio of the principal hemeII−CO photolysis bands at 1931 and 1907 cm^{-1} did not vary during the experiment or between nNOS samples. The peak/trough positions and line shape of the CO stretch features also did not change significantly between pH 6.5 and 8.6 (data not shown). The apparent ratios of CO bands in the photolysis experiments can be influenced by the kinetics of CO recombination and the quantum yield of CO photolysis. However, a comparison of the hemeII−CO ν_{C-O} stretch in the background-corrected absolute spectra (not shown) and the photolysis spectra shows no significant differences. Comparison of the two spectra shows that there is approximately a 10% steady-state level of CO dissociation under illumination. Fitting the difference spectra to Gaussian distributions gives a better fit if a small component (6%) is added at 1917.5 cm^{-1}. Good fits are given by pure Gaussian distributions centered at 1906.9, 1917.5, and 1931.4 cm^{-1} with bandwidths of 10.7, 9.0, and 15.4 cm^{-1} and 16%, 6%, and 78% of the area, respectively.

The spectra from 1800 to 1000 cm^{-1} contain changes in the protein backbone (amides I, II), prosthetic groups, and amino acid side chains (Figure 1). The region between 1700 and 1600 cm^{-1} in absolute spectra is normally dominated by amide I changes but includes many other vibrations. The amide I band in absolute spectra is 80% due to backbone C═O stretching. Features in the difference spectra are contributed by a limited subset of residues in or associated with the active site, which are significantly affected by CO binding. Two features are apparent centered at 1703 and 1688 cm^{-1} (peak/troughs at 1706/1700 and 1693/1685 cm^{-1}), which, in combination with the D_2O spectra and published vibrational data, can be tentatively assigned to heme propionate and the arginine guanidinium, respectively (below). Other major vibrations in this region (Figure 1) include a strong peak at 1668 cm^{-1}. Further peaks are observed at 1628 and 1610 cm^{-1} separated by a 1620 cm^{-1} trough.

In absolute spectra of proteins, the region around 1545 cm^{-1} is dominated by amide II vibrations which are 60% due to N−H bending and 40% due to C−N stretching; this region also contains potential cofactor and side chain vibrations. The amide II peak shifts from 1545 to 1445 cm^{-1} in D_2O; only a small feature is seen around 1445 cm^{-1} in the D_2O spectrum, so the contribution of the amide II band appears limited to only those backbone vibrations directly

Table 1: Major Bands in the nNOS FTIR CO Photolysis Difference Spectrum

H_2O suggested pair	D_2O	assignment	
		firm	tentative, possible
1931.3	1930.4	ν_{C-O}	
1906.5	1905.3	ν_{C-O}	
	Amide I Region		
1706/1700	1705/1693		heme propionate[a]
1693/1685	1625/1615		Arg $CN_3H_5^+$ ν_{as}[b]
1628/1620	1580/1570		Arg $CN_3H_5^+$ ν_s[b]
1610/1601			
	Amide II Region		
1596/1590			Arg COO^- ν_{as}[b]
1569/1554	*1580/1570*		Glut/Asp COO^- ν_{as}
1536	1537		
1519			
	Below 1500 cm^{-1}		
1428/1415/1396	1411		Glut/Asp COO^- ν_s, Arg COO^- ν_s[b]
1276/1266	1274/1261		
1254/1237/1220	1236		
1104/1096	1104/1092		
1057/1051	1056/1041		

[a] References: (*35*, *36*, *49*). [b] For review, see (*38*).

affected by CO photolysis. A prominent complex feature is observed with a distinct peak at 1569 cm^{-1}, a trough at 1536 cm^{-1}, and a peak at 1519 cm^{-1}.

Below 1500 cm^{-1}, a strong feature is observed with a peak at 1428 cm^{-1}, a trough at 1415 cm^{-1}, and a peak at 1396 cm^{-1}. Other distinct changes include features at 1276/1266, 1254/1235/1220, 1104/1096, and 1057/1051 cm^{-1}. All of these were consistently observed over six separate samples and three separate enzyme preparations.

Effects of H/D Exchange on CO Photolysis Difference Spectra. Shown in Figure 1B is a hemeII−CO photolysis difference spectrum of nNOS in D_2O at pD 7.6 and 283 K. The general form of the spectrum is similar to that observed in H_2O media, but there are significant differences. We used the amide II region of the absolute spectra to estimate the extent of D/H exchange following published methods (*31*, *32*); the exchange is above 85%.

D_2O induces a small shift to lower frequency, from 1931 to 1930 cm^{-1} for the principal trough, and from 1906 to 1905 cm^{-1} for the minor trough of the CO stretch. This small shift is at the limit of resolution in these spectra but is similar in magnitude to that reported by Jung et al. (*33*) for the heme domain of the iNOS isoform, although the peak positions are different. The spectrum is best fitted by three Gaussian components centered at 1905.7, 1917.5, and 1930.4 cm^{-1} with bandwidths of 12.5, 10.0, and 15.1 cm^{-1} and 19%, 8%, and 73% of the area, respectively.

In contrast to H_2O data, a single peak/trough is evident in the CO photolysis difference spectrum at 1705/1693 cm^{-1}. This is followed by a large peak and trough at 1665 and 1638 cm^{-1}, followed by a peak at 1625 cm^{-1}. Below 1600 cm^{-1}, a peak/trough is observed at 1580/1570 cm^{-1}. A marked trough is seen at 1537/1518 cm^{-1}, in a similar position to that observed in H_2O, but smaller. Below 1500 cm^{-1}, features are observed at 1430/1411/1398, 1274/1261, and 1236/1220 cm^{-1}. Below 1200 cm^{-1}, significant changes are observed at 1104/1092 and 1056/1041 cm^{-1}. The principal bands in the FTIR difference spectra, in both H_2O and D_2O media, are tabulated in Table 1.

Table 2: FTIR Spectra of Arginine[a]

Arginine Stretches		
	H_2O	D_2O
$CN_3H_5^+$ ν_{as}	1672 (450 M^{-1} cm^{-1})	1608 (460 M^{-1} cm^{-1})
	1691	*1600 (in proteins)*
$CN_3H_5^+$ ν_s	1635 (320 M^{-1} cm^{-1})	1586 (500 M^{-1} cm^{-1})
		1576 (in proteins)
NH_3^+ ν_{as}	1630 (200 M^{-1} cm^{-1})	~1176
NH_3^+ ν_s	1518 (180 M^{-1} cm^{-1})	−
COO^- ν_{as}	1595 (460 M^{-1} cm^{-1})	1590 (~800 M^{-1} cm^{-1})
COO^- ν_s	1414 (~300 M^{-1} cm^{-1})	1411 (~350 M^{-1} cm^{-1})
Tetrahydrobiopterin Vibrations		
	H_2O	D_2O
	1660	1645 *not paired*
	1607	1603
	1564	1576
	1359	
	1228	

[a] Shown in Figure 3 are FTIR spectra of H_4B in H_2O and D_2O media (*37*, *38*, and this paper). The spectra are absolute spectra of H_4B in TES buffer, pH/pD 7.6, with the buffer blank subtracted.

FTIR of the Prosthetic Groups and Arginine. The catalytic site of NOS contains H_4B, protoporphyrin IX, and, in the current case, arginine as substrate. The FTIR spectra of hemes (*35*, *36*) and arginine (*37*, *38*) have been reported. The principal infrared vibrations of arginine and H_4B are listed in Table 2. Unbound arginine has strongly absorbing vibrations: ν_{as} guanidinium at 1672 cm^{-1} (450 M^{-1} cm^{-1}) in H_2O and 1608 cm^{-1} (460 M^{-1} cm^{-1}) in D_2O; these can be shifted for arginine residues in proteins to about 1691 cm^{-1} in H_2O and 1600 cm^{-1} in D_2O (*37*, *38*). The ν_s for the unbound arginine guanidinium is at 1635 cm^{-1} (320 M^{-1} cm^{-1}) in H_2O and 1586 cm^{-1} (500 M^{-1} cm^{-1}) in D_2O. The latter shifts to 1576 cm^{-1} in protein in D_2O (no value available for H_2O) (*37*−*40*). In this study, the arginine is a ligand, not a residue; thus, the carboxylate and amino vibrations need to be considered. The amino $NH_3+\nu_{as}$ at 1630 cm^{-1} and $NH_3+\nu_s$ at 1518 cm^{-1} in water are relatively weak bands (approximately 200 M^{-1} cm^{-1}) (*37*). In Figure 3 the spectra of arginine and H_4B in both water and D_2O are shown; the spectra are corrected by subtraction of the solvent spectra. The spectrum of arginine in water is shown in Figure 3A. The spectrum is fitted for the guanidinium, carboxylate, and amino ν_{as} and ν_s; the CH_2 and CH fittings and some minor fillings are not shown in the figure. The fittings are 1675, 1640, 1631, 1600, 1519, and 1413 cm^{-1}, probably corresponding to guanidinium ν_{as} and ν_s, amino ν_{as}, carboxylate ν_{as}, amino ν_s, and carboxylate ν_s, respectively, and are close to the published data (Table 2). In D_2O (Figure 3B), the three expected components can fitted under the main peak and shoulder at 1616 and 1589 cm^{-1} (guanidinium ν_{as} and ν_s and carboxylate ν_{as}) although at slightly higher frequencies than the published data (putative guanidinium ν_{as} and ν_s at 1622 and 1615 cm^{-1} and carboxylate ν_{as} at 1597 cm^{-1}); the carboxylate ν_s is seen at 1411 cm^{-1} as expected (for clarity, only the non-overlapping carboxylate ν_s at 1411 cm^{-1} is shown). The amino $NH_3^+\nu_{as}$ and ν_s will undergo a large shift (approximately −400 cm^{-1}) in D_2O, but may be obscured in the region of 1200 cm^{-1} because of the difficulty in accurately subtracting the much larger D_2O solvent background, which absorbs very strongly at this frequency. The spectra of H_4B in H_2O and D_2O are shown in Figure

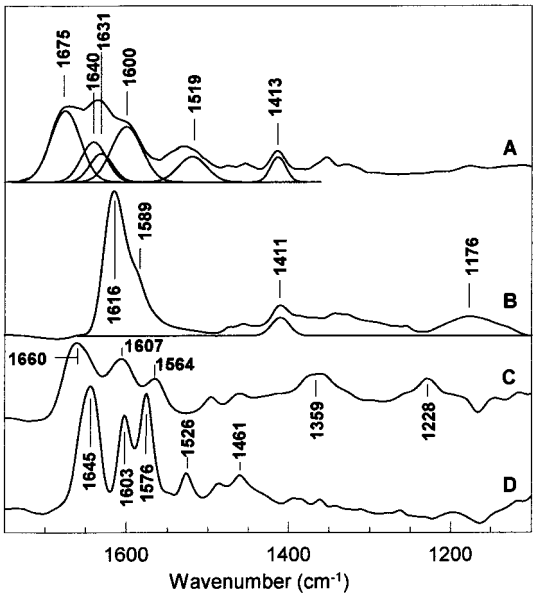

FIGURE 3: FTIR spectra of tetrahydrobiopterin and arginine. (A) Absorbance spectrum of L-arginine in water; (B) absorbance spectrum of L-arginine in D_2O; (C) H_4B in H_2O; (D) H_4B in D_2O. Absolute spectra of arginine were obtained from 0.5 M solutions in H_2O or D_2O at a pH/pD of 7.6; the spectra shown have the H_2O or D_2O control spectrum subtracted. Absolute spectra of H_4B dissolved in 400 mM TES buffer in either H_2O or D_2O were recorded and the spectra corrected for buffer by subtracting the spectra obtained for the buffers in the absence of H_4B. In all cases, 10 μL of solution was placed on a 25 mm diameter CaF_2 window, a second CaF_2 window was placed on top and squeezed, and the edges were sealed with Dow Corning MS24 Silicon Compound. Each spectrum is the product of 500 interferograms.

3C,D, respectively. H_4B vibrations are listed in Table 2 but not assigned or paired for H_2O/D_2O.

DISCUSSION

The HemeII−CO Stretch. HemeII−CO compounds of different hemoproteins have characteristic vibrations and bandwidths, and these have been reported for several high-spin heme enzymes including some NOS heme domains (tabulated in *35*). The ν_{C-O} stretches of native proteins are observed between 1905 and 1970 cm^{-1} with $\Delta\nu CO_{1/2}$ between 3 cm^{-1} (cytochrome *c* oxidase which is unusually narrow) and 15 cm^{-1}; multiple peaks are commonly observed (*35*). The position of the absorption will be influenced by the polarization of the CO molecule at the heme, and the spectrum can also be influenced by bending of the heme-CO by steric interactions. In general, hydrogen bonding of the CO to groups, including arginine, in the heme pocket will lower the stretching frequency, and contact with nonpolar residues will raise it. Conformations in which the Fe−C−O deviates from the normal will lower the stretching frequency, while, less likely, bending of the Fe−C−O will raise it (*41*).

Comparison of the heme pocket structures of NOS isoforms with arginine analogues bound is instructive, even though no crystal structure of a CO complex exists. Modeling CO into the pocket shows significant van der Waals overlap between arginine and CO bound as an axial heme ligand, with steric potential energies on the order of 10^6 kcal as estimated by Discover (MSI) with the CVFF force field (unpublished work). Torsion about the arginine Cδ−Nϵ bond can eliminate the steric overlap and repulsive potential at the cost of straining the hydrogen bonds provided by the conserved active site glutamate residue (E361 in iNOS); the tradeoff between the H-bonding and the steric constraints accounts for both the anticooperative binding of CO and arginine ($\Delta K_{eq} \sim 10-100$ at 298 K) and the interaction between the CO and arginine as observed in FTIR experiments. Similar effects can be obtained with alternative combinations of other torsions and translations of arginine within the ligand pocket, and small deviations in the Fe−C−O orientation from the heme normal are also expected as part of the adjustment in ligand binding modes in the ternary complex. While the effect on the stretching frequencies of CO is dominated by H-bond-like effects, the equilibrium is dominated by the steric overlap of the ligands in their preferred binding modes.

In NOS and cytochrome P-450s, substrates affect CO binding to the reduced heme and enhance its stability (*42*). The substrates cause the formation of a 'closed' structure in which the electron paramagnetic resonance spectra, resonance Raman spectra, FTIR, and CO-combination/recombination kinetics are affected, reflecting the fact that bound NO or CO is significantly restricted by the presence of substrate and some analogues (*33*, *43*−*47*). Resonance Raman spectra of the CO vibrations of nNOS and the influence of substrate have been reported (*44*). The hemeII−CO ν_{Fe-CO} and ν_{C-O} stretching frequencies are observed at ~502 and 1929 cm^{-1}, respectively, in the presence of substrate. In the absence of substrate, these bands are diminished, and additional species are observed at ~487 and 1949 cm^{-1}. Crystal structures provide a clear structural explanation; bound substrate covers the axial heme ligand binding position. This is not unexpected since oxygen chemistry in the initial step of the reaction requires the close approach of a terminal amino group of arginine to oxygen bound as an axial heme ligand. In addition to the kinetic barrier provided by arginine to CO binding and escape, CO and arginine binding are thermodynamically anticooperative, with CO raising the arginine K_d approximately 20-fold from about 50 nM (*48*).

The dominant ν_{C-O} stretch frequency we observe in the FTIR spectrum for the whole enzyme agrees with the published resonance Raman data for the nNOS isoform (*44*), but are different from the ν_{C-O} stretches seen in a detailed analysis of the iNOS isoform by FTIR (*33*). In the presence of arginine and H_4B, a spectrum is observed with an absorbance maximum at ~1905 cm^{-1} (298 K). In nNOS, we observe a minor 1907 cm^{-1} (difference spectrum) resonance, but the dominant species in nNOS is the 1931 cm^{-1} stretch. The ratio of the two features (1931/1907 cm^{-1}) is constant between preparations. The eNOS isoform, in the presence of arginine, also shows two features, at approximately 1904 and 1927 cm^{-1}; in this case, the 1904 cm^{-1} species is much more prominent (Ingledew, unpublished results). Our observations of the ν_{C-O} stretch in nNOS agree with the resonance Raman observations for the same isoform (*44*). Hence, there appear to be differences in the equilibrium between species with different FeC−O stretches between the enzyme's isoforms. We observe a shift of approximately 1 cm^{-1} in the peak position of the two principal CO stretches in D_2O compared to H_2O. A similar shift has been reported for iNOS, where it has been assigned to the presence of a hydrogen bond between the guanidinium group of the

arginine and the CO ligand (*33*) based on the FTIR measurements and consideration of the crystal structure (*17*).

Comparison of the crystal structures of NOS isoforms with arginine analogues bound reveals considerable flexibility in the ability of substituted arginines to bind in different positions relative to the heme while still making critical hydrogen bonds with conserved residues in the binding site; superimposition of the hemes reveals that the positions of H-bond donors and acceptors vary by 1−2 Å in different structures (*17*−*20*). The are no structures available which show simultaneous binding of CO and arginine in the ternary complex, but formation of the ternary complex is analogous to the binding of substituted arginines in which a steric challenge is posed against the binding mode of unsubstituted arginine. The steric overlap forces arginine into a less favorable binding mode which is reflected in the anticooperative binding of CO and arginine (*48*). The CO stretches will be altered directly by CO−arginine interaction and indirectly by the altered binding of CO. Modeling of simultaneous CO and arginine binding in NOS active sites suggests that in the presence of CO the principal interaction between the CO and the arginine will be through a terminal guanidinium nitrogen, and not through the associated protons.

In the CO photolysis spectrum of iNOS, a B-form of the ν_{C-O} stretch around 2140 cm^{-1} is reported (*33*); similar bands are present in nNOS spectra. Unbound CO does not have a significant vibration mode in this range; it can only be observed when bound. The observation of these B-states around 2140 cm^{-1} indicates that the CO must have a transient docking site that becomes occupied during photolysis and recombination from the heme (B-state). These B-states in iNOS are discussed by Jung and co-workers (*33*); they suggest, by analogy with myoglobin, that this state represents the CO staying close to the hemeII but almost parallel to the heme plane after photolysis. A spectrally similar 'B-state' is observed in cytochrome oxidase, but in this case the stretch (at 2062 cm^{-1}) is assigned to the photolyzed CO transiently binding to the CuI in the catalytic site (*25*). Adventious CuI could possibly give the same effect. Shown in Figure 2 are spectra obtained at different incubation times and their deconvolution. The ν_{C-O} stretches are altered in the aged ('P-420') enzyme. In the photolysis difference spectrum, its loss manifests as a trough with a minimum at 1967 cm^{-1}, and a peak is observed with a maximum at 1982 cm^{-1}. No absorbance around 2140 cm^{-1} is apparent, suggesting that in this form of the enzyme the photolyzed CO is not constrained to an orientation parallel to the heme plane but adopts a more perpendicular orientation on photolysis or recombination prior to relaxation to its original conformation; thus, a small spectral shift on photolysis gives the peak/trough feature observed. This 1982/1967 cm^{-1} feature correlates with the optically detected formation of the inactive 'P-420' form of the enzyme. As expected from previous work (*42*), its development is more rapid in the absence of arginine, and the long time course of experiments mitigates against obtaining good spectra of nNOS in the absence of substrate. This phenomenon and the protective effects of ligands are well documented in NOS; the P420 form is inactive, but the inactivation can be reversed (*34*, *42*). Another prominent feature of the 'P420' spectrum is a trough around 1545 cm^{-1}.

The Major FTIR Vibrations of Ligands and Prosthetic Groups. Crystal structures of the oxidized oxygenase domain have been reported for iNOS (*17*, *18*) and eNOS isoforms (*19*, *20*). From these structures, the residues involved in L-arginine and H_4B binding can be identified. A network of hydrogen bonds links the H_4B, glutamate E362 (eNOS numbering, putatively E592 in nNOS), the propionate group of the heme, and the guanidinium group of the arginine. In the reduced form, this network will be modified as arginine binds more tightly to the reduced enzyme and will be further modified in the presence of CO, which conflicts with arginine binding and may form a hydrogen bond to the arginine, as previously discussed.

In the photolysis difference spectrum, heme features may be expected to be present. FTIR and resonance Raman studies on porphyrins show complex spectra (*35*, *36*, *49*). Resonance Raman spectra of reduced nNOS have major vibrations at 1349 and 1359 cm^{-1} and minor features around 1466, 1422, 1388, 1219, 1172, and 1127 cm^{-1}; the Fe oxy-form has major features at 1372 and 1132 cm^{-1} (*23*). Resonance Raman spectra of the oxy-compound of hemoglobin show major features at 1599, 1342, 1305, 1225, 1133, and 756 cm^{-1} (reviewed in *36*). FTIR of reduced cytochrome b_{559} shows principle heme reduction related vibrations at 1685, 1545, and 1239 cm^{-1} (*49*). However, we are interested primarily in those vibrations which are different in the CO-ligated and non-CO-ligated ferrous hemes, and data on this are currently difficult to extract. In model compounds, comparing the FeII meso-porphyrin with one pyridine ligand against the same but with an additional CO ligand (Figure 3 in *27*) indicates bands in the difference spectrum would be found at around 1740 cm^{-1} (this probably corresponds to the protonated propionate). In addition, small changes are clustered around 1450 and 1250 cm^{-1}, a peak/trough can be deduced at 1170 cm^{-1}, and further differences are indicated around 1100 cm^{-1}. Essentially similar differences are observed when comparing the same two forms of the deuterioporphyrin. A resonance Raman study of hemoglobin and myoglobin shows differences between the non-CO-ligated and CO-ligated forms at 1605 (appearance of unligated) and 1630 cm^{-1} (loss of ligated) (*36*); if these transitions are detected by FTIR, they cannot be readily seen in the spectra. In this study, only the propionate stretch, 1705 cm^{-1}, can be currently (tentatively) assigned.

Comparison of the FTIR Spectra in H_2O and D_2O Media. Figure 4 compares the H_2O (spectrum A) and D_2O (spectrum B) spectra and their difference spectrum (spectrum A−B) expanded in the region from 1750 to 1500 cm^{-1}. In the H_2O sample, two CO-photolysis-induced features are clearly resolved with maxima/minima at 1706/1700 cm^{-1} and 1693/1685 cm^{-1}, respectively. These most likely correspond to the propionate side chain of the heme and the ν_{as} of the arginine guanidinium, respectively (Table 2 and references cited therein). On deuteration, the heme propionate would be expected to shift approximately 3 cm^{-1} lower; such a shift is observed from a center at 1703 cm^{-1} to a center at 1698 cm^{-1} [the former value will be distorted by overlap with the 1693/1685 cm^{-1} species, so the extent of the shift is approximately as reported for other hemoproteins (*49*, *50*)]. The ν_{as} for the arginine guanidinium will shift approximately (−)65 cm^{-1} in D_2O. The shift for the unbound arginine guanidinium is 1672 cm^{-1} (H_2O) to 1608 cm^{-1} (D_2O), but in proteins, the residue is seen at 1688−1695 cm^{-1} (H_2O) shifting to 1595−1605 cm^{-1} (D_2O) (*39*, *40*). This is

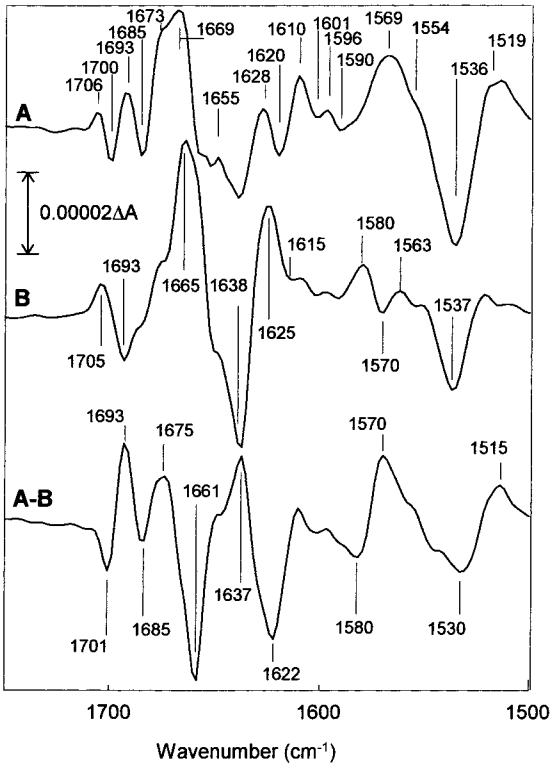

FIGURE 4: Comparison of the light-induced FTIR difference spectrum in H_2O and D_2O (1750−1500 cm^{-1}) at pH/pD 7.6 and 283 K. (A) Light *minus* dark difference spectrum in H_2O from which 50% of the dark *minus* dark control has been subtracted. (B) Light *minus* dark difference spectrum in D_2O from which 50% of the dark *minus* dark control has been subtracted. (A−B) The double difference spectrum taken by subtraction of spectrum B from spectrum A after normalization of the magnitude of their major hemeII−CO stretch. Samples of the CO adduct of fully reduced nNOS were prepared in H_2O and D_2O buffers as described under Materials and Methods; the spectra were obtained as described in the legend of Figure 1.

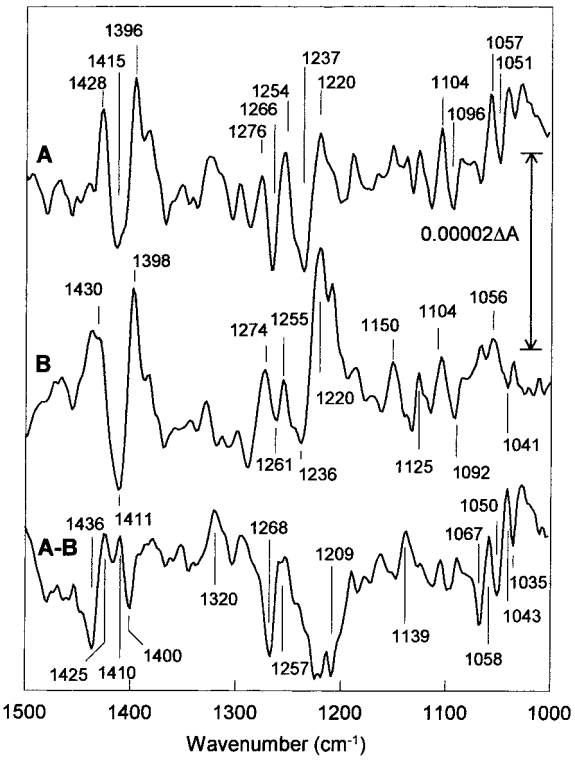

FIGURE 5: Comparison of the light-induced FTIR difference spectrum in H_2O and D_2O (1500−1000 cm^{-1}) at pH/pD 7.6 and 283 K. (A) Light *minus* dark difference spectrum in H_2O from which 50% of the dark *minus* dark control has been subtracted. (B) Light *minus* dark difference spectrum in D_2O from which 50% of the dark *minus* dark control has been subtracted. (A−B) The double difference spectrum taken by subtraction of spectrum B from spectrum A after normalization of their major hemeII−CO stretches. Samples of the CO adduct of fully reduced nNOS were prepared in H_2O and D_2O buffers as described under Materials and Methods; the spectra were obtained as described in the legend of Figure 1.

compatible with the data; the 1693/1685 cm^{-1} peak/trough is not seen in D_2O, and a new band with a peak/trough at 1625/1615 cm^{-1} is present. A ν_s resonance is expected for the guanidinium around 1633 cm^{-1} in H_2O, shifting to around 1586−1577 cm^{-1} in D_2O. There is a feature (1628 cm^{-1}) in the H_2O spectrum and a corresponding change in the D_2O and difference spectra with a peak/trough at 1580/1570 cm^{-1} which may be due to the guanidinium ν_s (D_2O). Substrate arginine has a carboxyl and an amino group which also need to be considered. Peptide amino groups have ν_{as} and ν_s at 1630 and 1518 cm^{-1} (relatively low extinction coefficient, ~200 M^{-1} cm^{-1}) which undergo a shift to lower frequency of several hundred wavenumbers in D_2O, and more strongly absorbing carboxyl groups which have ν_{as} and ν_s at 1595 and 1414 cm^{-1}, shifting, in D_2O, to 1590 and 1411 cm^{-1}, respectively (Table 2). These features may be present, but the extinction coefficients are relatively low, and more work is required before they can be assigned with confidence.

The major trough at 1537 cm^{-1} (H_2O) is in approximately the same place in H_2O and D_2O. It is smaller in the latter; this is exaggerated by the loss of the adjacent 1569/1554 cm^{-1} peak/shoulder on the high-wavenumber side and diminution of the peak at 1519 cm^{-1} on the low-wavenumber side. The diminution of the feature can only be partly assigned to loss of the amide II feature (N−H) which shifts to approximately 1445 cm^{-1} in D_2O because only a small additional feature is see in the D_2O spectra at around 1445 (trough at 1436 cm^{-1} in Figure 5 A−B). Another candidate for the 1569/1554 cm^{-1} species is the conserved glutamate or aspartate COO^- ν_{as}, which in D_2O would be expected to shift to 1567 cm^{-1} [Glut COO^- ν_{as}, H_2O: 1558 cm^{-1}, 460 M^{-1} cm^{-1}; D_2O: 1567 cm^{-1}, 830 M^{-1} cm^{-1}, (*37*)]. Changes are seen in these positions in the respective solvents (the 1569/1554 cm^{-1} species moving to 1580/1570 cm^{-1}); a caveat is that the ν_s for the arginine guanidinium may also occupy the 1580/1570 cm^{-1} vibration in D_2O. Tyrosine residues have a characteristic sharp major feature (ring vibration) at ~1513 cm^{-1} (~1517 cm^{-1} in D_2O), and although tyrosines are conserved in the catalytic core, no assignment can be made in this overlapped region without additional information (e.g., from work with site-directed mutants). For clarity, the double difference spectrum (H_2O−D_2O) is also shown in Figure 4.

Figure 5 compares the H_2O (spectrum A) and D_2O (spectrum B) spectra and their difference spectrum expanded in the region from 1500 to 1000 cm^{-1}. The peak/trough/peak around 1415 cm^{-1} (H_2O) is seen to shift slightly in D_2O. This is the standard position for a ν_s of a carboxyl group. The prime candidates are the conserved glutamate or aspartate residues or the carboxyl of the bound arginine (or all of these), since none of the prosthetic groups have major bands in this region (*37*). A trough/peak around 1237/1220 cm^{-1} is seen in both spectra, but there are significant

differences around 1255−1274 cm^{-1}. A 1104/1092−6 cm^{-1} feature is seen in both spectra, but there are differences in the region of 1057/1051 cm^{-1}. Some of the vibrations in this low-frequency region may be due to heme, but there may be other contributions (e.g., tyrosine, and in D_2O the arginine $NH_3+\nu_{as}$).

CONCLUSIONS

We report putative vibrational bands of ligands, prosthetic groups, and protein and amino acid side chains in nNOS using FTIR. D_2O exchange has been used to give difference spectra to facilitate assignments, probing the fine structure at the catalytic site. The spectra have been interpreted in light of known atomic structures, with some tentative assignments being made. The assignments need to be confirmed by a combination of isotopic and site-directed mutagenesis studies and the ligation of substrate analogues and inhibitors.

ACKNOWLEDGMENT

We thank Miles Lyon for expert technical assistance.

REFERENCES

1. Ignarro, L. J., Buga, G. M., Wood, K. S., Byrns, R. E., and Chadhuri, G. (1987) *Proc. Natl. Acad. Sci. U.S.A. 84*, 9265−9269.
2. Palmer, R. M. J., Ferringe, D. S., and Moncada, S. (1987) *Nature 327*, 524−526.
3. Furchgott, R. F. (1988) *Vasoldilation: Vascular Smooth Muscle, Peptides, Autonomic Nerves and Endothelium*, pp 401−404, Raven Press, New York.
4. Moncada, S., Palmer, R. M., and Higgs, E. A. (1989) *Biochem. Pharmacol. 38*, 1709−1715.
5. Ignarro, L. J. (1990) *Annu. Rev. Pharmacol. Toxicol. 30*, 535−560.
6. Nathan, C., and Xie, Q. W. (1994) *J. Biol. Chem. 269*, 13725−13728.
7. MacMicking, J., Xie, Q. W., and Nathan, C. (1997) *Annu. Rev. Immunol. 15*, 323−350.
8. Griffith, O. W., and Stuehr, D. J. (1995) *Annu. Rev. Physiol. 57*, 707−736.
9. Hibbs, J. B., Taintor, R. R., and Vavrin, Z. (1987) *Science 235*, 473−476.
10. Marletta, M. A. (1993) *J. Biol. Chem. 268*, 12231−12234.
11. Stuehr, D. J. (1991) *J. Biol. Chem. 266*, 6259−6263
12. Ghosh, D. K., Abu-Soud, H. M., and Stuehr, D. J. (1996) *Biochemistry 35*, 1444−1449.
13. Sheta, E. A., McMillan, K., and Masters, B. S. (1994) *J. Biol. Chem. 269*, 15147−15153.
14. Ghosh, D. K., and Stuehr, D. J. (1995) *Biochemistry 34*, 801−807.
15. Bredt, D. S., Hwang, P. M., Glatt, C. E., Lowenstein, C., Reed, R. R., and Snyder, S. H. (1991) *Nature 351*, 714−718.
16. Sheta, E. A., McMillan, K., and Masters, B. S. S. (1994) *J. Biol. Chem. 269*, 15147−15153.
17. Crane, B. R., Rosenfeld, R. J., Arvai, A. S., Ghosh, D. K., Ghosh, S., Tainer, J. A., Stuehr, D. J., and Getzoff, E. D. (1999) *EMBO J. 18*, 6271−6281.
18. Li, H., Raman, C. S., Glaser, C. B., Blasko, E., Young, T. A., Parkinson, J. F., Whitlow, M., and Poulos, T. L. (1999) *J. Biol. Chem. 274*, 21276−21284.
19. Raman, C. S., Li, H., Martasek, P., Krial, V., Masters, B. S., and Poulos, T. L. (1998) *Cell 95*, 939−950.
20. Fischmann, T. O., Hruza, A., Da Niu, X., Fossetta, J. D., Lunn, C. A., Dolphin, E., Prongay, A. J., Reichart, P., Lundell, D., Narula, S. K., and Weber, P. C. (1999) *Nat. Struct. Biol. 6*, 233−242.
21. Siddhanta, U., Presta, A., Fan, B., Wolan, D., Rousseau, D. L., and Stuehr, D. J. (1998) *J. Biol. Chem. 273*, 18950−18958.
22. Abu-Soud, H. M., Wang, J., Rousseau, D. L., and Stueher, D. J. (1999) *Biochemistry 38*, 12446−12451.
23. Couture, M., Stuehr, D. J., and Rousseau, D. L. (2000) *J. Biol. Chem. 275*, 3201−3205.
24. Couture, M., Adak, S., Stuehr, D. J., and Rousseau, D. L. (2001) *J. Biol. Chem. 276*, 38280−38288.
25. Alben, J. O., Moh, P. P., Flamingo, F. G., and Altschuld, R. A. (1981) *Proc. Natl. Acad. Sci. U.S.A. 78*, 234−237.
26. Mitchell, D. M., Shapleigh, J. P., Archer, A. M., Alben, J. O., and Gennis, R. B. (1996) *Biochemistry 35*, 9446−9450.
27. Park, S., Pan, L. P., Chan, S. I., and Alben, J. O. (1996) *Biophys. J. 71*, 1036−1047.
28. Rich, P. R., and Breton, J. (2001) *Biochemistry 40*, 6441−6449.
29. Hall, A. V., Antoniou, H., Wang, Y., Cheung, A. H., Arbus, A. M., Olson, S. L., Lu, W. C., Kau, C. L., and Marsden, P. A. (1994) *J. Biol. Chem. 269*, 33082−33090.
30. Downer, N. W., Bruchman, T. J., and Hazzard, J. H. (1986) *J. Biol. Chem. 261*, 3640−3647.
31. Rath, P., DeGrip, W. J., and Rothschild, J. (1998) *Biophys. J. 74*, 192−198.
32. McMillan, K., Bredt, D. S., Hirsch, D. J., Snyder, S. H., Clark, J. E., and Masters, B. S. (1992) *Proc. Natl. Acad. Sci. U.S.A. 89*, 11141−11145.
33. Jung, C., Stuehr, D. J., and Ghosh, D. K. (2000) *Biochemistry 39*, 10167−10171.
34. Huang, L. X., Abu-Soud, H. M., Hille, R., and Stuehr, D. J. (1999) *Biochemistry 38*, 1912−1920.
35. Alben, J. O. (1978) in *The Porphyrins* (Dolphin, D., Ed.) Vol. III, pp 323−393, Academic Press, New York.
36. Felton, R. H., and Yu, N.-T. (1978) in *The Porphyrins* (Dolphin, D., Ed.) Vol. III, p 347, Academic Press, New York.
37. Venyaminov, S. Y., and Kalnin, N. N. (1990) *Biopolymers 30*, 1243−1257.
38. Barth, A. (2000) *Prog. Biophys. Mol. Biol. 74*, 141−173.
39. Berendzen, J., and Braunstein, D. (1990) *Proc. Natl. Acad. Sci. U.S.A. 87*, 1−5.
40. Rudiger, M., Haupts, U., Gerwert, K., and Oesterhelt, P. (1995) *EMBO J. 14*, 1599−1606.
41. Balasubramanian, S., Lambright, D. G., and Boxer, S. (1993) *Proc. Natl. Acad. Sci. U.S.A. 90*, 4718−4722.
42. Jung, C., Hoa, G. H. B., Schroder, K. L., and Douchet, J. P. (1992) *Biochemistry 31*, 12855−12862.
43. Migita, C. T., Salerno, J. C., Masters, B. S. S., Martasek, P., McMillan, K., and Ikeda Saito, M. (1997) *Biochemistry 36*, 10987−10992.
44. Wang, J., Stuehr, D. J., and Rousseau, D. L. (1997) *Biochemistry 36*, 4595−4606.
45. Scheele, J. S., Kharitonov, V. G., Martasek, P., Roman, L. J., Sharma, V. S., Masters, B. S., and Magde, D. (1997) *J. Biol. Chem. 272*, 12523−12528.
46. Matsuoka, A., Stuehr, D. J., Olson, J. S., Clark, P., and Ikeda-Saito, M. (1994) *J. Biol. Chem. 269*, 20335−30339.
47. Abu-Soud, H. M., Wu, C., Ghosh, D. K., and Stuehr, D. J. (1998) *Biochemistry 37*, 3777−3786.
48. Smith, S. M. E., and Salerno, J. C. (2000) *Nitric Oxide J. 4*, 224.
49. Berthomieu, B., Boussac, A., Mantele, W., Breton, J., and Naberdryk, E. (1992) *Biochemistry 31*, 11460−11471.
50. Puustinen, A., Bailey, J. A., Dyer, R. B., Mecklenburg, S. L., Wickstrom, M., and Woodruff, W. H. (1997) *Biochemistry 36*, 13195−13200.

BI012101V